Journal of Materials Chemistry C

ROYAL SOCIETY OF CHEMISTRY

PAPER

Cite this: DOI: 10.1039/d5tc04474j

Ionic gating of a *meta*-connected molecular junction achieves a 10^5 ON/OFF ratio

Faizah Almutairi,†[a] Asma Alajmi,†[ab] Colin Lambert [a] and Ali Ismael *[ac]

Received 22nd December 2025,
Accepted 3rd March 2026

DOI: 10.1039/d5tc04474j

rsc.li/materials-c

Molecular architectures featuring stable radical centres and tunable π-conjugated backbones are well-established platforms for investigating charge transport at the single-molecule level. In this study, we examine the transport characteristics of three established connectivities *para*-connected, *ortho*-connected, and doubly π-bridged *ortho* based on bis(triarylamine) organic analogues, in the presence of counter-ions positioned at various locations around the molecular framework. These systems provide a platform for assessing how structural connectivity governs quantum interference and how local electrostatic perturbations influence the transmission spectrum. Building on these benchmarks, a new *meta*-connected variant is proposed and its behaviour in the presence of counter ions is evaluated. In contrast to the *para* and *ortho* arrangements, which display only modest variations under ionic perturbation, the *meta* configuration exhibits a markedly enhanced response. Depending on the ion's position, the transmission is either significantly suppressed or strongly modulated by nearly five orders of magnitude producing an ON/OFF ratio of $\sim 10^5$. This pronounced switching arises from the destructive interference inherent to *meta* connectivity and its susceptibility to local electrostatic fields. Overall, the results demonstrate that *meta*-engineered molecular junctions offer a highly sensitive route for ion gated control of charge transport, with promising implications for molecular scale electronic switching and sensing technologies.

1. Introduction

Electron transport through organic molecules[1–5] is governed by quantum interference even at room temperature. Consequently, interfering pathways available for electrons within a molecular framework play a crucial role in determining the efficiency and characteristics of charge transport.[6–12] In recent years, considerable attention has been directed toward exploiting quantum interference (QI) effects as a strategy for modulating electrical conductance at the single-molecule level. At the same time, π-conjugated molecular systems[13–19] continue to attract strong interest, as their delocalized electronic structures provide a versatile platform for tailoring transport properties. This growing focus reflects broader advancements in molecular electronics and related research fields, where controlling electron flow with precision has become a central objective.

In a single-molecule junction (SMJ), the molecular backbone acts as the principal medium for electron transfer between the two metallic electrodes. Quantum interference arises when electrons traverse multiple transmission pathways within a molecule, whether through spatially separated routes or through frontier molecular orbitals.[20–27] The relative phase relationship between these pathways determines whether constructive quantum interference (CQI) or destructive quantum interference (DQI) occurs, resulting in enhanced or suppressed conductance, respectively. Charge transport in SMJs is influenced by several molecular and interfacial factors, including the chemical nature of the anchoring groups, the molecular length, the characteristics of the spacer units, and the electronic structure of the π-conjugated framework. Aromatic systems, particularly those with *para*, *ortho*, or double-*ortho* connectivities[28–35] are especially sensitive to QI effects, as variations in connectivity reconfigure the available phase-coherent pathways within the conjugated network. Understanding these principles has enabled the design of functional molecular devices,[36–41] including molecular wires,[42,43] switches,[44] and thermoelectric elements.[45–49] Substitution patterns, conformational flexibility, and modifications to anchoring geometries further influence the energy alignment and interference patterns, thereby providing additional means to control charge-transport behaviour in π-conjugated molecular systems. Building on these developments, theoretical frameworks such as density functional theory (DFT) and tight-binding (i.e. Hückel) models have become indispensable for analysing charge transport in π-conjugated systems. By correlating electronic structure with observed conductance trends, these

[a] Physics Department, Lancaster University, Lancaster, LA1 4YB, UK
[b] Department of Physics, College of Science and Humanities in Al-Kharj, Prince Sattam Bin Abdulaziz University, Al-Kharj 11942, Saudi Arabia
[c] Department of Physics, College of Education for Pure Science, Tikrit University, Tikrit, Iraq. E-mail: k.ismael@lancaster.ac.uk
† These authors contributed equally to this work.

models play a central role in interpreting experimental measurements and in predicting how targeted chemical modifications can be used to control electron transport in single-molecule junctions.

In this study, we investigate how different connectivity patterns within molecular systems shown in Fig. 1 govern charge transport in single-molecule junctions. The *para*-connected configuration Fig. 1(a) provides an extended continuous π-conjugation pathway, which generally promotes phase-coherent electron transport and is expected to lead to high electrical conductance. In contrast, the single-bridge *ortho*-connected system in Fig. 1(b) is expected to reduce orbital overlap, thereby suppressing electron transmission. Incorporating a double-bridge *ortho*-connected system in Fig. 1(c) is expected to improve electron transport compared with the single-bridged *ortho* case Fig. 1(b). In what follows, we test these expectations through detailed DFT-based transport calculations. Molecular connectivity plays a central role in controlling QI and charging transport in single-molecule junctions. In π-conjugated systems, *para*- and *ortho*-connected architectures typically support relatively robust transport pathways, whereas *meta* connectivity introduces DQI that strongly suppresses transmission near the Fermi energy. This interference-driven sensitivity makes *meta*-connected junctions particularly responsive to external electrostatic perturbations, such as nearby counter-ions. Ionic gating therefore provides an effective means to modulate molecular conductance without modifying the molecular backbone. Understanding the interplay between connectivity-induced QI and ion-induced electrostatic effects is essential for the rational design of molecular switches, sensors, and thermoelectric devices.[50,51]

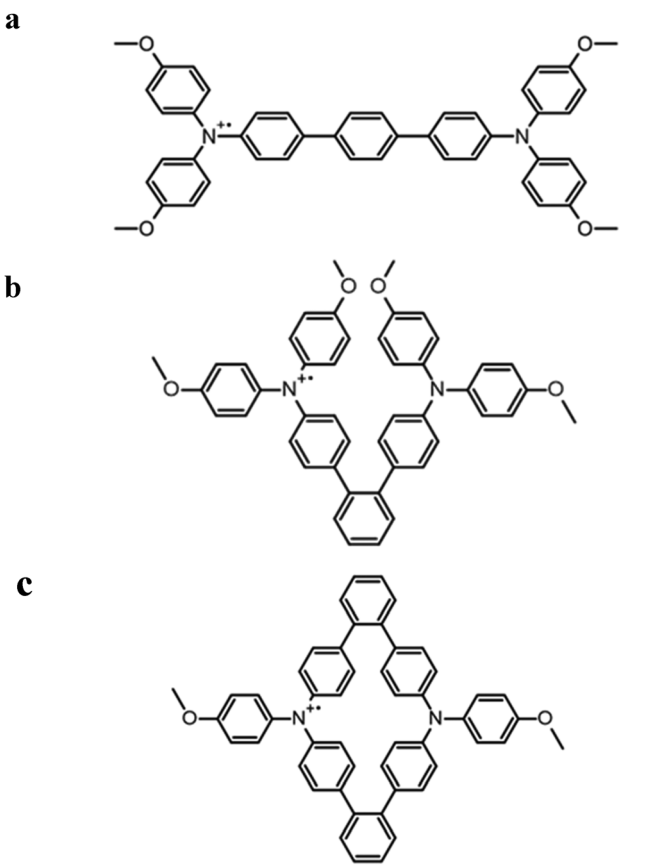

Fig. 1 Chemical structures of the studied molecular systems: (a) *para*-connected, (b) *ortho*-connected, and (c) doubly π-bridged *ortho*.

2. Computational methods

Density functional theory calculations were performed using the SIESTA package.[52–56] The geometries of the isolated molecules were fully optimised by allowing all atomic coordinates to relax until the residual forces on each atom were below 0.01 eV $Å^{-1}$ A double-ζ polarized DZP basis set was employed together with norm-conserving pseudopotentials, and the real-space integration grid was defined using a cutoff energy of 250 Ry. Exchange correlation effects were treated within the generalized gradient approximation GGA. The geometries obtained from DFT optimisations were then employed as input structures for the quantum transport calculations. The fully relaxed molecular configurations used in the transport analysis are presented in Fig. S2 of the SI, highlighting the characteristic conformations of each system. In addition, their electronic properties were evaluated through frontier molecular orbital (FMO) analysis examining the highest orbital molecule orbital (HOMO), lowest orbital molecule orbital (LUMO), and adjacent orbitals as shown in Fig. S3–S5. The frontier molecular orbitals provide insight into the spatial distribution of amplitude and phase that governs charge transport and QI phenomena. Each molecule incorporates two terminal methoxy groups as anchoring units. To evaluate their transport properties, we employed the non-equilibrium Green's function (NEGF) Gollum quantum transport code. This framework enables calculation of the energy dependent transmission coefficient $T(E)$, which quantifies the ease with which an electron of energy E can traverse the junction. The corresponding electrical conductance is then obtained from the Landauer expression, $G = G_0T(E_F)$[57–60] where G_0 is the quantum of conductance. For all simulations, the molecules were connected between two semi-infinite gold electrodes represented by six-layer Au(111) slabs, each comprising 30 atoms. The methoxy anchors were placed on the gold surfaces in their most energetically favorable adsorption geometries to reflect experimentally realistic binding configurations.

3. Results and discussion

3.1. DFT calculations

This section examines the electrical conductance characteristics of three molecular systems: the *para*-connected analogue Fig. 1(a), the single-bridge *ortho*-connected species Fig. 1(b), and the *ortho*-connected double-bridge system Fig. 1(c). Using DFT optimised geometries as input, we investigate how this distinct connectivity pattern shape QI behaviour within the molecular framework. We begin by analysing how each connection pattern gives rise to DQI or CQI signatures in the

charge-transport pathways. We then assess their thermoelectric properties through Seebeck coefficient calculations, highlighting how CQI and DQI influence both conductance and overall thermoelectric performance.

3.2. Connectivity analysis

As discussed above, the double-bridge design Fig. 1(c) partially restores conjugation and is therefore expected to yield higher conductance than the single-bridge *ortho* system Fig. 1(b), while remaining less conductive than the fully conjugated *para*-linked structure Fig. 1(a) (for more detail about the electronic properties see Fig. S1–S5, in the SI). To evaluate these qualitative predictions, we analyse the DFT-calculated transmission functions for the bridged molecular systems. As a preliminary step, binding-energy calculations were performed for the methoxy (OCH_3)–gold contacts.[60–63] These results confirm that the anchoring configurations are consistent across all molecules. The optimised Au–OCH_3 bond lengths and binding energies Fig. S6 confirm the formation of stable and reproducible methoxy–gold junctions across all molecules. Binding energies were evaluated using a pyramidal gold configuration to mimic an STM or break-junction apex, while a planar model though slightly underestimating the binding energy by ~0.8 eV provides a robust geometry for assessing the intrinsic transport properties of the molecular backbone. Fig. 2(a)–(c) present the electrode molecule geometries employed in the transport simulations for the three systems. The corresponding $T(E)$, are shown in Fig. 2(d) as a function of electron energy relative to the DFT-predicted Fermi level, E_F^{DFT}. For each connectivity, the transmission curves represent averages over four different counter-ion positions; the individual configurations and their detailed analysis are provided in the SI. All three systems exhibit smooth transmission functions within the HOMO-LUMO gaps, which is a signature of CQI. The *para*-connected molecule Fig. 2(a) displays the highest transmission coefficient in the vicinity of the middle of the gap, reflecting the presence of a strongly conjugated transport pathway. In contrast, the *ortho*-connected structure Fig. 2(b) exhibits the lowest mid-gap transmission, consistent with a less efficient π-conjugation pathway. The doubly π-bridged *ortho* architecture Fig. 2(c) shows intermediate behavior, with enhanced transmission relative to the single-ortho system but remaining lower than that of the *para*-connected analogue. This trend indicates that the introduction of a second π-bridge partially improves through-molecule coupling, although it does not fully recover the high conjugation efficicy of the *para* configuration Fig. 2(a).

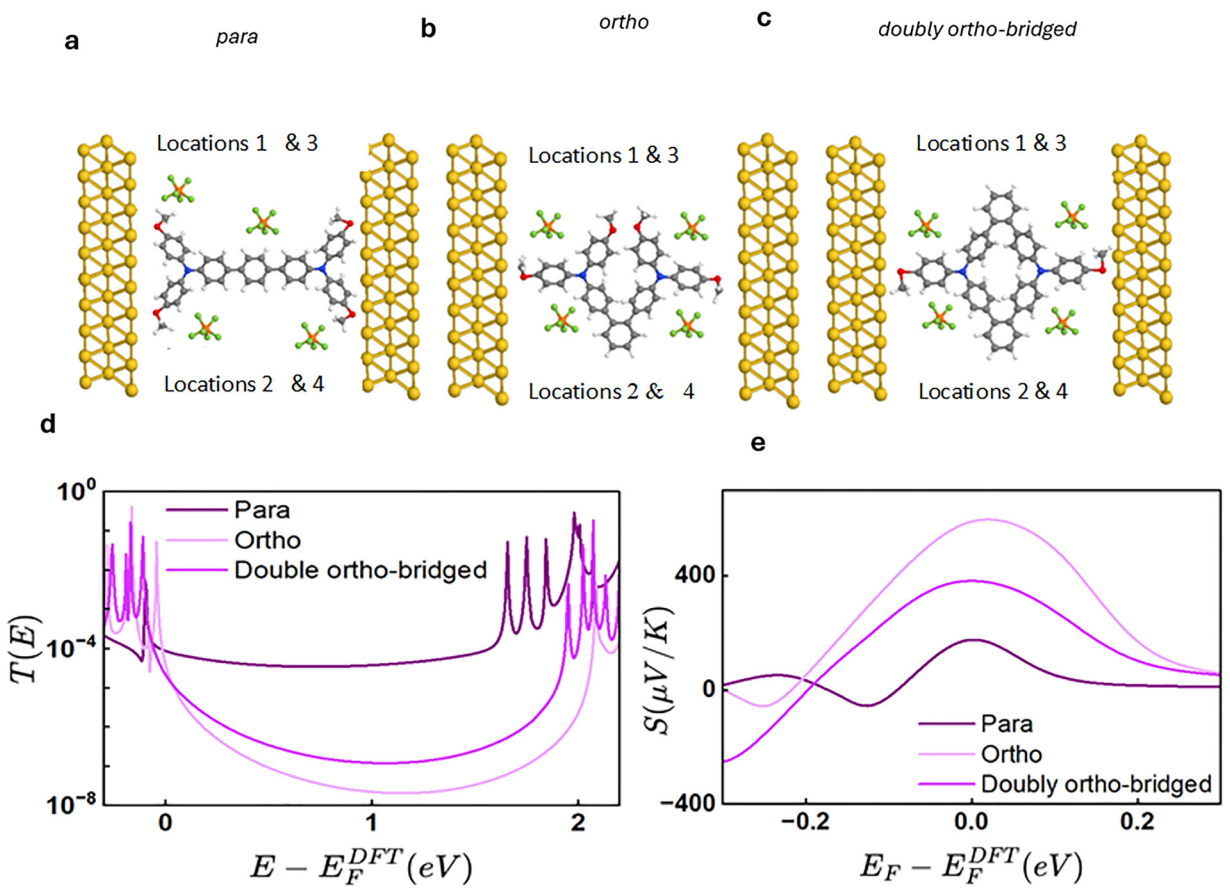

Fig. 2 (a)–(c) Relaxed junction geometries of the para-connected molecule (a) single-bridge ortho-connected molecule (b) and doubly π-bridged ortho-connected molecule (c) coupled to gold electrodes *via* terminal methoxy (OCH_3) anchoring groups. (d) Zero-bias average transmission coefficients, $T(E)$, plotted as a function of electron energy relative to the DFT-predicted Fermi energy E_F^{DFT}. (e) average Seebeck coefficients, $S(E)$, plotted as a function of Fermi energy relative to the DFT-predicted Fermi energy E_F^{DFT}.

At the DFT Fermi energy, the average transmission coefficients are 7.4×10^{-5} for the *para*-connected system, 2.5×10^{-6} for the doubly π-bridged *ortho* system, and 7.7×10^{-7} for the *ortho*-connected system, confirming the expected hierarchy of conductances. Additional details, including the full transmission coefficient curves, are presented in Fig. S7–S9 of the SI. Further details of the spin-polarized transport calculations and charge transfer analysis, including the spin-resolved transmission spectra (Fig. S19) and population analysis for different PF_6^- counter-ion positions (Table S1), are provided in the SI.

3.3. Seebeck coefficient

The Seebeck coefficient $S(E_F)$ is particularly important because a temperature gradient ΔT across a molecular junction can induce an electrical potential ΔV according to $\Delta V = -S(E_F)\Delta T$.[64–66] A large $S(E_F)$ therefore indicates a strong ability of a molecule to convert heat into electrical energy without the need for any mechanical components. When the transmission function has an approximately linear slope over an energy window on the order of k_BT around the Fermi level E_F, the Seebeck coefficient can be estimated using the Mott relation:

$$S(E_F) = -\frac{\pi^2 k_B{}^2 T}{3e}\frac{\partial \ln T(E)}{\partial E}\bigg|_{E=E_F}$$

For each molecular connectivity, the Seebeck coefficients shown in Fig. 2(e) are averaged over four distinct counter-ion positions; the individual configurations and detailed analyses are provided in the SI. As shown in Fig. 2(d), the $T(E)$ exhibit a negative slope in the vicinity of the Fermi energy E_F for all connectivities. According to the Mott relation, this negative slope implies a positive Seebeck coefficient, consistent with the Seebeck trends observed in Fig. 2(e) and indicative of HOMO-dominated transport.

Because the Seebeck coefficient is proportional to the energy derivative of $\ln T(E)$evaluated at E_F, the Mott relation provides a straightforward estimate of $S(E_F)$ for each connectivity.[66] Applying this relation to the calculated transmission slopes predicts that the *para*-connected molecule Fig. 2(a) exhibits the smallest thermopower, the doubly *ortho*-bridged structure Fig. 2(c) shows an intermediate value, and the single-bridge *ortho*-connected molecule Fig. 2(c) yields the largest Seebeck coefficient. Notably, this ordering is opposite to the corresponding conductance trend: the lowest-conductance junction displays the highest thermopower, whereas the most conductive structure exhibits the weakest Seebeck response. Additional details and full Seebeck curves are provided in Fig. S10–S12 of the SI.

These trends are reflected in the computed thermopower values for the molecular series. The *ortho*-connected junction shows a Seebeck coefficient of approximately +600 μV K^{-1}, the *para*-connected structure yields a smaller value of about +160 μV K^{-1}, and the doubly-ortho configuration falls between them at roughly +300 μV K^{-1}. This behaviour highlights how the connectivity-dependent interference pattern shapes the energy profile of the transmission function, which *via* Mott formula, then converts into the corresponding seebeck response.

3.4. New suggested molecule, *meta*-connected

To further probe the role of connectivity, we extend our analysis by constructing a *meta*-connected analogue shown in Fig. 3, in which the phenyl ring in the centre of the bridge is *meta*-connected to its neighbours (for more details about the electronic structure of this molecule see Fig. S13–S15 in the SI).

The *meta*-arrangement interrupts the through-bond conjugation pathway and is expected to give rise to DQI, leading to a markedly suppressed transmission within the HOMO-LUMO gap. The calculated zero-bias transmission for the *meta*-connected molecule reaches a minimum of approximately 4.7×10^{-8}, significantly lower than that of the *para*, *ortho*, and doubly-*ortho* structures Fig. 2(a)–(c). This pronounced DQI not only reduces the conductance but also steepens the energy dependence of $T(E)$, which results in an enhanced thermopower relative to the other connectivities. Consistent with the large negative slope of $\ln T(E)$ at E_F, the *meta*-connected system exhibits the highest Seebeck coefficient in the series, reaching more than +750 μV K^{-1}. This strong thermoelectric response highlights how interference-driven suppression of transmission can amplify the Seebeck coefficient, in accordance with the Mott relation. A complete depiction of the *meta*-connected molecular geometry is presented in Fig. 4(a), while detailed analyses including the optimised structures, frontier orbitals, transmission spectra $T(E)$, and corresponding Seebeck profiles $S(E_F)$ illustrated in Fig. 4(c), are provided in the SI (Fig. S16 and S17). Together, these results demonstrate that even small adjustments in atomic connectivity can profoundly alter QI patterns and, consequently, the charge- and heat-transport characteristics of π-conjugated molecular systems.

3.5. On-Off ratio

To evaluate how local electrostatic perturbations influence charge transport, we performed simulations on all four of the above molecular junctions in the presence of PF_6 counterions. For molecules Fig. 2(a)–(c), the presence and position of the counterions produced only minor variations in $T(E)$, indicating that these architectures are relatively insensitive to local gating due to their robust π-delocalisation and CQI.[67–72] In contrast, the *meta*-connected molecule is highly sensitive to counterion perturbations that break symmetry within the π-system. These results reveal a pronounced switch-like ON/OFF response in the *meta*-connected system. Depending on the location of the counterion, Fig. 5 shows that two clearly separated transmission regimes are identified. In the low-conductance state, the

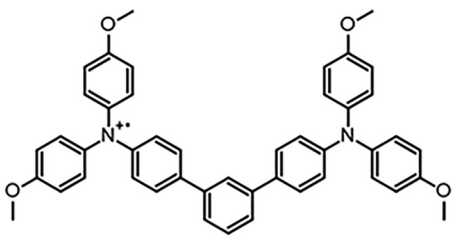

Fig. 3 Chemical structure of the *meta*-connected configuration.

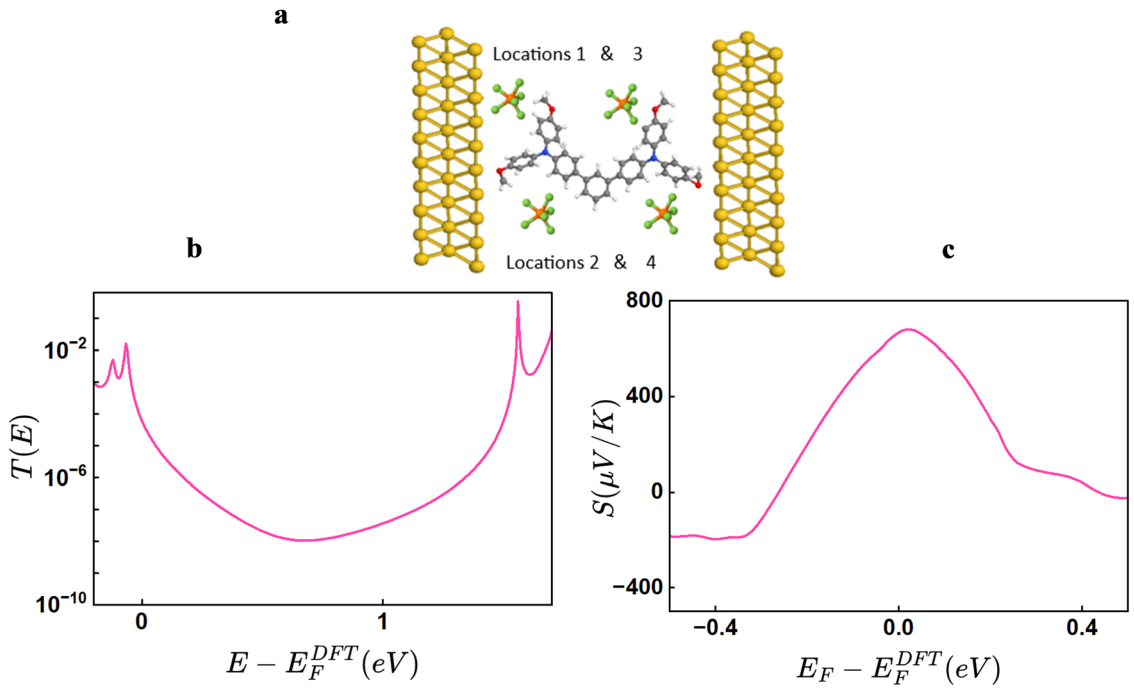

Fig. 4 (a) schematic of the meta-connected junction. (b) average transmission $T(E)$of the meta-connected molecular for four ion positions. (c) corresponding average Seebeck coefficient $S(E_F)$.

transmission is strongly suppressed, with $T(E)$ reduced by several orders of magnitude relative to the transmission in Fig. 4 (*i.e.* in the absence of counterions). This suppression arises from ion-induced perturbations of the molecular electronic structure that reinforce DQI, thereby inhibiting electron transport. In contrast, the high-conductance state exhibits a substantial enhancement of transmission, approaching an increase of approximately five orders of magnitude. This enhancement reflects a partial lifting of DQI and an improved effective conjugation across the junction, driven by ion-induced shifts in the energy alignment between molecular orbitals and the electrode Fermi level. As shown in Fig. 5(a), the coexistence of these two transmission levels demonstrates that the *meta*-connected architecture functions as an electrostatically gated interference switch, in which modest spatial variations in ion position toggle the junction between OFF and ON states. Such pronounced sensitivity is absent in the other molecular connectivities studied, highlighting the *meta* pathway as a uniquely promising platform for molecular switching, electrostatic gating, and charge-sensing applications.[73,74]

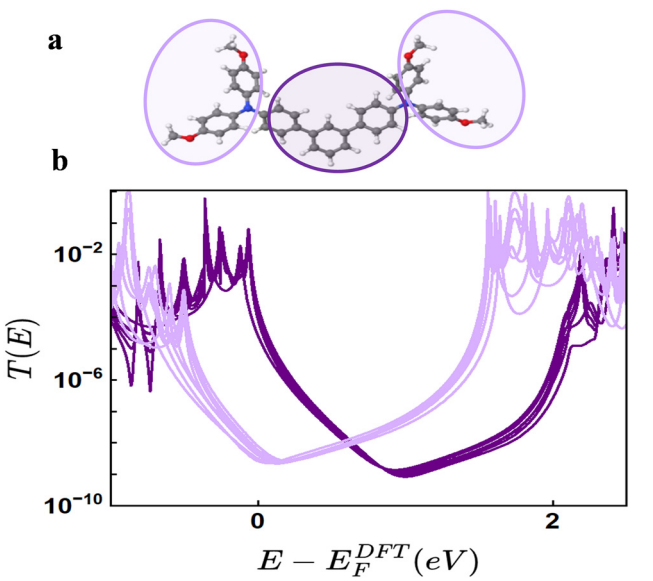

Fig. 5 (a) Schematic of the corresponding locations. (b) Transmission $T(E)$ of the *meta*-connected molecular for 20 counter-ion positions. Methoxy near the anchors suppress transmission (OFF), while central placement enhances it (ON), giving an ON/OFF ratio of $\sim 10^5$.

Conclusion

In conclusion, this study demonstrates that the *meta*-connectivity in radical-based molecular junctions provides a uniquely sensitive platform for electrostatic gating, in stark contrast to more robust *para* and *ortho* arrangements. By exploiting the inherent destructive quantum interference of the *meta* backbone, the strategic placement of a single counter ion enables modulation of the transmission spectrum by nearly five orders of magnitude, achieving an impressive ON/OFF ratio of $\sim 10^5$. This pronounced switching behavior underscores the critical role of molecular connectivity in determining interference patterns and their susceptibility to local electrostatic perturbations. These findings establish *meta*-engineered architectures as highly promising candidates for applications in molecular-scale electronic switches and ultrasensitive chemical sensors.

Conflicts of interest

There are no conflicts to declare.

Data availability

In this work, we use the following codes: Siesta code used to predict the Hamiltonian of each system used in this study, which is located in https://gitlab.com/siesta-project/siesta/-/releases. GOLLUM software is used to find the website's transmission coefficient. https://www.gollumcode.com/. Conductance, Seebeck, and other parameters are calculated using the own Fortran code available upon request.

Supplementary information (SI): The SI provides Optimised DFT structures of isolated molecules, Binding energy, Transmission coefficient $T(E)$, Seebeck coefficient S, New suggested meta-connected molecule, Spin-polarized calculations and Charge transfer analyses. See DOI: https://doi.org/10.1039/d5tc04474j.

Acknowledgements

This work was supported by the UK EPSRC (grant QMol EP/X026876/1). A. K. I. acknowledges the Leverhulme Trust for Early Career Fellowship ECF-2020-638. A. K. I. acknowledge financial support from the Tikrit University (Iraq), and the Iraqi Ministry of Higher Education (SL-20). F. A., and A. A. are grateful for financial assistance from Shagra University, and Prince Sattam bin Abdulaziz University, Al-Kharj.

References

1 K. Yoshizawa, An Orbital Rule for Electron Transport in Molecules, *Acc. Chem. Res.*, 2012, **45**(9), 1612–1621, DOI: 10.1021/ar300075f.

2 C. J. Lambert, Basic Concepts of Quantum Interference and Electron Transport in Single-Molecule Electronics, *Chem. Soc. Rev.*, 2015, **44**(4), 875–888, DOI: 10.1039/C4CS00203B.

3 V. Coropceanu, J. Cornil, D. A. Da Silva Filho, Y. Olivier, R. Silbey and J.-L. Brédas, Charge Transport in Organic Semiconductors, *Chem. Rev.*, 2007, **107**(4), 926–952, DOI: 10.1021/cr050140x.

4 F.-R. F. Fan, J. Yang, L. Cai, D. W. Price, S. M. Dirk, D. V. Kosynkin, Y. Yao, A. M. Rawlett, J. M. Tour and A. J. Bard, Charge Transport through Self-Assembled Monolayers of Compounds of Interest in Molecular Electronics, *J. Am. Chem. Soc.*, 2002, **124**(19), 5550–5560, DOI: 10.1021/ja017706t.

5 S. Pan, Q. Fu, T. Huang, A. Zhao, B. Wang, Y. Luo, J. Yang and J. Hou, Design and Control of Electron Transport Properties of Single Molecules, *Proc. Natl. Acad. Sci. U. S. A.*, 2009, **106**(36), 15259–15263, DOI: 10.1073/pnas.0903131106.

6 J. A. J. Burton, M. J. Edwards, D. J. Richardson and T. A. Clarke, Electron Transport Across Bacterial Cell Envelopes, *Annu. Rev. Biochem.*, 2025, **94**(1), 89–109, DOI: 10.1146/annurev-biochem-052621-092202.

7 P. A. Derosa and J. M. Seminario, Electron Transport through Single Molecules: Scattering Treatment Using Density Functional and Green Function Theories, *J. Phys. Chem. B*, 2001, **105**(2), 471–481, DOI: 10.1021/jp003033+.

8 O. Seitz, T. Böcking, A. Salomon, J. J. Gooding and D. Cahen, Importance of Monolayer Quality for Interpreting Current Transport through Organic Molecules: Alkyls on Oxide-Free Si, *Langmuir*, 2006, **22**(16), 6915–6922, DOI: 10.1021/la060718d.

9 A.-K. Singh, K. Martin, M. Mastropasqua Talamo, A. Houssin, N. Vanthuyne, N. Avarvari and O. Tal, Single-Molecule Junctions Map the Interplay between Electrons and Chirality, *Nat. Commun.*, 2025, **16**(1), 1759, DOI: 10.1038/s41467-025-56718-9.

10 S. J. K. O'Neill, M. Ashizawa, A. M. McLean, R. R. Serrano, T. Shimura, M. Agetsuma, M. Tsutsumi, T. Nemoto, C. D. J. Parmenter, J. A. McCune, G. G. Malliaras, N. Matsuhisa and O. A. Scherman, Supramolecular Conductive Hydrogels With Homogeneous Ionic and Electronic Transport, *Adv. Mater.*, 2025, **37**(26), 2415687, DOI: 10.1002/adma.202415687.

11 K. Kimura, R. Tamaki, M. Lee, X. Ouyang, S. Kusaba, R. B. Jaculbia, Y. Kawada, J. Jung, A. Muranaka, H. Imada, I. Katayama, J. Takeda and Y. Kim, Ultrafast On-Demand Exciton Formation in a Single-Molecule Junction by Tailored Terahertz Pulses, *Science*, 2025, **387**(6738), 1077–1082, DOI: 10.1126/science.ads2776.

12 A. K. Ismael, I. Grace and C. J. Lambert, Increasing the Thermopower of Crown-Ether-Bridged Anthraquinones, *Nanoscale*, 2015, **7**(41), 17338–17342, DOI: 10.1039/C5NR04907E.

13 P. Samorí, X. Feng and D. Bonifazi, π-Conjugated Molecules: From Structure to Function, *ChemPlusChem*, 2019, **84**(9), 1177–1178, DOI: 10.1002/cplu.201900442.

14 S. Ito and K. Tanaka, π-Conjugated Polymers Consisting of Heavier Group 13 Elements, *Polym. Chem.*, 2025, **16**(18), 2046–2057, DOI: 10.1039/D5PY00116A.

15 A. Mateo-Alonso, π-Conjugated Materials: Here, There, and Everywhere, *Chem. Mater.*, 2023, **35**(4), 1467–1469, DOI: 10.1021/acs.chemmater.2c03567.

16 K. Sakaushi and H. Nishihara, Two-Dimensional π-Conjugated Frameworks as a Model System to Unveil a Multielectron-Transfer-Based Energy Storage Mechanism, *Acc. Chem. Res.*, 2021, **54**(15), 3003–3015, DOI: 10.1021/acs.accounts.1c00172.

17 T. Kubo, Syntheses and Properties of Open-Shell π-Conjugated Molecules, *Bull. Chem. Soc. Jpn*, 2021, **94**(9), 2235–2244, DOI: 10.1246/bcsj.20210224.

18 N. Fukui, Skeletal Transformation of π-Conjugated Molecules for Functional Materials, *Bull. Chem. Soc. Jpn.*, 2025, **98**(7), uoaf062.

19 A. A. Al-Jobory and A. K. Ismael, Controlling Quantum Interference in Tetraphenyl-Aza-BODIPYs, *Curr. Appl. Phys.*, 2023, **54**, 1–4, DOI: 10.1016/j.cap.2023.06.004.

20 F. S. Kim, G. Ren and S. A. Jenekhe, One-Dimensional Nanostructures of π-Conjugated Molecular Systems: Assembly, Properties, and Applications from Photovoltaics, Sensors, and Nanophotonics to Nanoelectronics, *Chem. Mater.*, 2011, **23**(3), 682–732, DOI: 10.1021/cm102772x.

21 L. Zang, Y. Che and J. S. Moore, One-Dimensional Self-Assembly of Planar π-Conjugated Molecules: Adaptable Building Blocks for Organic Nanodevices, *Acc. Chem. Res.*, 2008, **41**(12), 1596–1608, DOI: 10.1021/ar800030w.

22 Y. Takeda, Modulating the Photophysical Properties of Twisted Donor–Acceptor–Donor π-Conjugated Molecules: Effect of Heteroatoms, Molecular Conformation, and Molecular Topology, *Acc. Chem. Res.*, 2024, **57**(15), 2219–2232, DOI: 10.1021/acs.accounts.4c00353.

23 Y. Zhang, H. Luo, S. Zhang, L. Huang, L. Cao, X. Dong and G. Zou, Halide Ion-Directed Symmetry Control in π-Conjugated Molecular Crystals, *Inorg. Chem.*, 2025, **64**(25), 12874–12880, DOI: 10.1021/acs.inorgchem.5c02303.

24 A. Khasbaatar, Z. Xu, J.-H. Lee, G. Campillo-Alvarado, C. Hwang, B. N. Onusaitis and Y. Diao, From Solution to Thin Film: Molecular Assembly of π-Conjugated Systems and Impact on (Opto)Electronic Properties, *Chem. Rev.*, 2023, **123**(13), 8395–8487, DOI: 10.1021/acs.chemrev.2c00905.

25 P. S. Fernando, Y.-C. Chen, J. M. Baek and Y. Diao, Chiral Assemblies of π-Conjugated Molecules: Fundamentals, Processing Strategies, and Applications in (Opto)Electronics, *Annu. Rev. Chem. Biomol. Eng.*, 2025, **16**(1), 59–91, DOI: 10.1146/annurev-chembioeng-100722-104224.

26 F. J. M. Hoeben, P. Jonkheijm, E. W. Meijer and A. P. H. J. Schenning, About Supramolecular Assemblies of π-Conjugated Systems, *Chem. Rev.*, 2005, **105**(4), 1491–1546, DOI: 10.1021/cr030070z.

27 A. K. Ismael, L. Rincón-García, C. Evangeli, P. Dallas, T. Alotaibi, A. A. Al-Jobory, G. Rubio-Bollinger, K. Porfyrakis, N. Agraït and C. J. Lambert, Exploring Seebeck-Coefficient Fluctuations in Endohedral-Fullerene, Single-Molecule Junctions, *Nanoscale Horiz.*, 2022, **7**(6), 616–625, DOI: 10.1039/D1NH00527H.

28 J. Wang, P. Zhang, C. Wang, X. Zheng, Y. Zhao, L. Li and S. Miao, Band Structure Tunable Synthesis of Photocatalytic Porous Aromatic Frameworks *via* Scholl Reaction, *Mater. Des.*, 2020, **186**, 108371, DOI: 10.1016/j.matdes.2019.108371.

29 G. Comas-Vilà and P. Salvador, Capturing Electronic Substituent Effect with Effective Atomic Orbitals, *Phys. Chem. Chem. Phys.*, 2025, **27**(20), 10482–10491, DOI: 10.1039/D5CP01299F.

30 A. Yamane, S. Fujii and T. Nishino, Geometry-Dependent Suppression of Quantum Interference in Thiolate- and Nitrile-Terminated Naphthalene Junctions, *ACS Omega*, 2025, **10**(36), 42102–42108, DOI: 10.1021/acsomega.5c08235.

31 L. Ge, S. Hou, Y. Chen, Q. Wu, L. Long, X. Yang, Y. Ji, L. Lin, G. Xue, J. Liu, X. Liu, C. J. Lambert, W. Hong and Y. Zheng, Hydrogen-Bond-Induced Quantum Interference in Single-Molecule Junctions of Regioisomers, *Chem. Sci.*, 2022, **13**(33), 9552–9559, DOI: 10.1039/D2SC03229E.

32 S. Fujii, A. Yamane, H. Goto and T. Nishino, Impact of π-Electron Delocalization on Quantum Interference in Single-Molecule Junctions of Benzene Derivatives, *Phys. Chem. Chem. Phys.*, 2025, **27**(45), 24412–24418, DOI: 10.1039/D5CP03176A.

33 K. Alresheedi, A. Alajmi, A. Alrehaili, A. Al-Jobory, C. Lambert and A. Ismael, Orientational Control of Quantum Interference in Ferrocene Single-Molecule Junctions, *Mater. Chem. Front.*, 2025, **9**(20), 3044–3050, DOI: 10.1039/D5QM00487J.

34 B. Alanazi, A. Alajmi, A. Aljobory, C. Lambert and A. Ismael, Tuning Quantum Interference through Molecular Junctions Formed from Cross-Linked OPE-3 Dimers, *J. Mater. Chem. C*, 2024, **12**(19), 6905–6910, DOI: 10.1039/D4TC00611A.

35 A. Mateo-Alonso, π-Conjugated Materials: Here, There, and Everywhere, *Chem. Mater.*, 2023, **35**(4), 1467–1469, DOI: 10.1021/acs.chemmater.2c03567.

36 M. B. Avinash and T. Govindaraju, Architectonics: Design of Molecular Architecture for Functional Applications, *Acc. Chem. Res.*, 2018, **51**(2), 414–426, DOI: 10.1021/acs.accounts.7b00434.

37 C. Zhang, Y. Yan, Y. S. Zhao and J. Yao, From Molecular Design and Materials Construction to Organic Nanophotonic Devices, *Acc. Chem. Res.*, 2014, **47**(12), 3448–3458, DOI: 10.1021/ar500192v.

38 P. M. Beaujuge and J. M. J. Fréchet, Molecular Design and Ordering Effects in π-Functional Materials for Transistor and Solar Cell Applications, *J. Am. Chem. Soc.*, 2011, **133**(50), 20009–20029, DOI: 10.1021/ja2073643.

39 N. Yang, S. Zhang, Y. Cui, J. Wang, S. Cheng and J. Hou, Molecular Design for Low-Cost Organic Photovoltaic Materials, *Nat. Rev. Mater.*, 2025, **10**(6), 404–424, DOI: 10.1038/s41578-025-00792-4.

40 L. Sun, Y. A. Diaz-Fernandez, T. A. Gschneidtner, F. Westerlund, S. Lara-Avila and K. Moth-Poulsen, Single-Molecule Electronics: From Chemical Design to Functional Devices, *Chem. Soc. Rev.*, 2014, **43**(21), 7378–7411, DOI: 10.1039/C4CS00143E.

41 M. Alshammari, A. A. Al-Jobory, T. Alotaibi, C. J. Lambert and A. Ismael, Orientational Control of Molecular Scale Thermoelectricity, *Nanoscale Adv.*, 2022, **4**(21), 4635–4638, DOI: 10.1039/D2NA00515H.

42 W.-Y. Lo, N. Zhang, Z. Cai, L. Li and L. Yu, Beyond Molecular Wires: Design Molecular Electronic Functions Based on Dipolar Effect, *Acc. Chem. Res.*, 2016, **49**(9), 1852–1863, DOI: 10.1021/acs.accounts.6b00305.

43 C. Zhang, Y. Yan, Y. S. Zhao and J. Yao, From Molecular Design and Materials Construction to Organic Nanophotonic Devices, *Acc. Chem. Res.*, 2014, **47**(12), 3448–3458, DOI: 10.1021/ar500192v.

44 J. L. Zhang, J. Q. Zhong, J. D. Lin, W. P. Hu, K. Wu, G. Q. Xu, A. T. S. Wee and W. Chen, Towards Single Molecule Switches, *Chem. Soc. Rev.*, 2015, **44**(10), 2998–3022, DOI: 10.1039/C4CS00377B.

45 H. Chen and J. Fraser Stoddart, From Molecular to Supramolecular Electronics, *Nat. Rev. Mater.*, 2021, **6**(9), 804–828, DOI: 10.1038/s41578-021-00302-2.

46 Y. Zhao, M. Gobbi, L. E. Hueso and P. Samorì, Molecular Approach to Engineer Two-Dimensional Devices for CMOS and beyond-CMOS Applications, *Chem. Rev.*, 2022, **122**(1), 50–131, DOI: 10.1021/acs.chemrev.1c00497.

47 X.-L. Shi, N.-H. Li, M. Li and Z.-G. Chen, Toward Efficient Thermoelectric Materials and Devices: Advances, Challenges, and Opportunities, *Chem. Rev.*, 2025, **125**(16), 7525–7724, DOI: 10.1021/acs.chemrev.5c00060.

48 A. K. Ismael and C. J. Lambert, Molecular-Scale Thermoelectricity: A Worst-Case Scenario, *Nanoscale Horiz.*, 2020, **5**(7), 1073–1080, DOI: 10.1039/D0NH00164C.

49 D. Zheng, J. Zhang, S. Sun, J. Liang, Y. Li, J. Luo and D. Liu, Flexible Organic Thermoelectric Composites and Devices with Enhanced Performances through Fine-Tuning of Molecular Energy Levels, *ACS Appl. Electron. Mater.*, 2024, **6**(6), 4754–4763, DOI: 10.1021/acsaelm.4c00796.

50 X. Li, Z. Xu, D. Bu, J. Cai, H. Chen, Q. Chen, T. Chen, F. Cheng, L. Chi, W. Dong, Z. Dong, S. Du, Q. Fan, X. Fan, Q. Fu, S. Gao, J. Guo, W. Guo, Y. He, S. Hou, Y. Jiang, H. Kong, B. Li, D. Li, J. Li, Q. Li, R. Li, S. Li, Y. Lin, M. Liu, P. Liu, Y. Liu, J. Lü, C. Ma, H. Pan, J. Pan, M. Pan, X. Qiu, Z. Shen, S. Tan, B. Wang, D. Wang, L. Wang, L. Wang, T. Wang, X. Wang, X. Wang, X. Wang, Y. Wang, Y. Wang, K. Wu, W. Xu, N. Xue, L. Yan, F. Yang, Z. Yang, C. Zhang, X. Zhang, Y. Zhang, Y. Zhang, X. Zhou, J. Zhu, Y. Zhang, F. Gao and Y. Wang, Recent Progress on Surface Chemistry I: Assembly and Reaction, *Chin. Chem. Lett.*, 2024, **35**(12), 110055, DOI: 10.1016/j.cclet.2024.110055.

51 X. Li, Z. Xu, D. Bu, J. Cai, H. Chen, Q. Chen, T. Chen, F. Cheng, L. Chi, W. Dong, Z. Dong, S. Du, Q. Fan, X. Fan, Q. Fu, S. Gao, J. Guo, W. Guo, Y. He, S. Hou, Y. Jiang, H. Kong, B. Li, D. Li, J. Li, Q. Li, R. Li, S. Li, Y. Lin, M. Liu, P. Liu, Y. Liu, J. Lü, C. Ma, H. Pan, J. Pan, M. Pan, X. Qiu, Z. Shen, Q. Sun, S. Tan, B. Wang, D. Wang, L. Wang, L. Wang, T. Wang, X. Wang, X. Wang, X. Wang, Y. Wang, Y. Wang, K. Wu, W. Xu, N. Xue, L. Yan, F. Yang, Z. Yang, C. Zhang, X. Zhang, Y. Zhang, Y. Zhang, X. Zhou, J. Zhu, Y. Zhang, F. Gao and Y. Wang, Recent Progress on Surface Chemistry II: Property and Characterization, *Chin. Chem. Lett.*, 2025, **36**(1), 110100, DOI: 10.1016/j.cclet.2024.110100.

52 V. Blum, R. Gehrke, F. Hanke, P. Havu, V. Havu, X. Ren, K. Reuter and M. Scheffler, Ab Initio Molecular Simulations with Numeric Atom-Centered Orbitals, *Comput. Phys. Commun.*, 2009, **180**(11), 2175–2196, DOI: 10.1016/j.cpc.2009.06.022.

53 D. Nozaki, H. Sevinçli, W. Li, R. Gutiérrez and G. Cuniberti, Engineering the Figure of Merit and Thermopower in Single-Molecule Devices Connected to Semiconducting Electrodes, *Phys. Rev. B*, 2010, **81**(23), 235406, DOI: 10.1103/PhysRevB.81.235406.

54 M. Seidl, J. P. Perdew and S. Kurth, Simulation of All-Order Density-Functional Perturbation Theory, Using the Second Order and the Strong-Correlation Limit, *Phys. Rev. Lett.*, 2000, **84**(22), 5070–5073, DOI: 10.1103/PhysRevLett.84.5070.

55 J. M. Soler, E. Artacho, J. D. Gale, A. García, J. Junquera, P. Ordejón and D. Sánchez-Portal, The SIESTA Method for Ab Initio Order- N Materials Simulation, *J. Phys.: Condens. Matter*, 2002, **14**(11), 2745–2779, DOI: 10.1088/0953-8984/14/11/302.

56 D. Nozaki, H. Sevinçli, W. Li, R. Gutiérrez and G. Cuniberti, Engineering the Figure of Merit and Thermopower in Single-Molecule Devices Connected to Semiconducting Electrodes, *Phys. Rev. B*, 2010, **81**(23), 235406, DOI: 10.1103/PhysRevB.81.235406.

57 J. Liu, X. Huang, F. Wang and W. Hong, Quantum Interference Effects in Charge Transport through Single-Molecule Junctions: Detection, Manipulation, and Application, *Acc. Chem. Res.*, 2019, **52**(1), 151–160, DOI: 10.1021/acs.accounts.8b00429.

58 T. Markussen, R. Stadler and K. S. Thygesen, The Relation between Structure and Quantum Interference in Single Molecule Junctions, *Nano Lett.*, 2010, **10**(10), 4260–4265, DOI: 10.1021/nl101688a.

59 A. K. Ismael, A. Al-Jobory, I. Grace and C. J. Lambert, Discriminating Single-Molecule Sensing by Crown-Ether-Based Molecular Junctions, *J. Chem. Phys.*, 2017, **146**(6), 064704, DOI: 10.1063/1.4975771.

60 L. Li, J. Z. Low, J. Wilhelm, G. Liao, S. Gunasekaran, C. R. Prindle, R. L. Starr, D. Golze, C. Nuckolls, M. L. Steigerwald, F. Evers, L. M. Campos, X. Yin and L. Venkataraman, Highly Conducting Single-Molecule Topological Insulators Based on Mono- and Di-Radical Cations, *Nat. Chem.*, 2022, **14**(9), 1061–1067, DOI: 10.1038/s41557-022-00978-1.

61 K. Yoshida, F. Takasaki, M. Uebe, S. Seki and A. Ito, Impact of Double-π-Bridge on Bis(Triarylamine)-Based Organic Mixed-Valence System: A Case Study of Diaza[1.1](4,4″) Ortho -Terphenylophane Radical Cation, *Chem. – Eur. J.*, 2025, **31**(6), e202403945, DOI: 10.1002/chem.202403945.

62 L. Li, S. Louie, N. M. Orchanian, C. Nuckolls and L. Venkataraman, Long-Range Gating in Single-Molecule One-Dimensional Topological Insulators, *J. Am. Chem. Soc.*, 2024, **146**(24), 16920–16925, DOI: 10.1021/jacs.4c05699.

63 Y. Wang, Y.-J. Hu, B. Bocklund, S.-L. Shang, B.-C. Zhou, Z.-K. Liu and L.-Q. Chen, First-Principles Thermodynamic Theory of Seebeck Coefficients, *Phys. Rev. B*, 2018, **98**(22), 224101, DOI: 10.1103/PhysRevB.98.224101.

64 M. Hong, W. Lyu, Y. Wang, J. Zou and Z.-G. Chen, Establishing the Golden Range of Seebeck Coefficient for Maximizing Thermoelectric Performance, *J. Am. Chem. Soc.*, 2020, **142**(5), 2672–2681, DOI: 10.1021/jacs.9b13272.

65 X. Wang, A. Ismael, B. Alanazi, A. Al-Jobory, J. Wang and C. J. Lambert, High Seebeck Coefficient from Isolated Oligo-Phenyl Arrays on Single Layered Graphene *via* Stepwise Assembly, *J. Mater. Chem. C*, 2023, **11**(42), 14652–14660, DOI: 10.1039/D3TC02842A.

66 Q. H. Al-Galiby, H. Sadeghi, D. Z. Manrique and C. J. Lambert, Tuning the Seebeck Coefficient of Naphthalenediimide by Electrochemical Gating and Doping, *Nanoscale*, 2017, **9**(14), 4819–4825, DOI: 10.1039/C7NR00571G.

67 C. J. Lambert, Basic Concepts of Quantum Interference and Electron Transport in Single-Molecule Electronics, *Chem. Soc. Rev.*, 2015, **44**(4), 875–888, DOI: 10.1039/C4CS00203B.
68 R. Frisenda, V. A. E. C. Janssen, F. C. Grozema, H. S. J. Van Der Zant and N. Renaud, Mechanically Controlled Quantum Interference in Individual π-Stacked Dimers, *Nat. Chem.*, 2016, **8**(12), 1099–1104, DOI: 10.1038/nchem.2588.
69 J. Liu, X. Huang, F. Wang and W. Hong, Quantum Interference Effects in Charge Transport through Single-Molecule Junctions: Detection, Manipulation, and Application, *Acc. Chem. Res.*, 2019, **52**(1), 151–160, DOI: 10.1021/acs.accounts.8b00429.
70 T. Markussen, R. Stadler and K. S. Thygesen, The Relation between Structure and Quantum Interference in Single Molecule Junctions, *Nano Lett.*, 2010, **10**(10), 4260–4265, DOI: 10.1021/nl101688a.
71 T. Markussen, R. Stadler and K. S. Thygesen, The Relation between Structure and Quantum Interference in Single Molecule Junctions, *Nano Lett.*, 2010, **10**(10), 4260–4265, DOI: 10.1021/nl101688a.
72 G. C. Solomon, D. Q. Andrews, T. Hansen, R. H. Goldsmith, M. R. Wasielewski, R. P. Van Duyne and M. A. Ratner, Understanding Quantum Interference in Coherent Molecular Conduction, *J. Chem. Phys.*, 2008, **129**(5), 054701, DOI: 10.1063/1.2958275.
73 Y.-P. Li, H.-R. Yang, Q. Zhao, W.-C. Song, J. Han and X.-H. Bu, Ratiometric and Selective Fluorescent Sensor for Zn^{2+} as an ''Off–On–Off'' Switch and Logic Gate, *Inorg. Chem.*, 2012, **51**(18), 9642–9648, DOI: 10.1021/ic300738e.
74 A. Borges, J. Xia, S. H. Liu, L. Venkataraman and G. C. Solomon, The Role of Through-Space Interactions in Modulating Constructive and Destructive Interference Effects in Benzene, *Nano Lett.*, 2017, **17**(7), 4436–4442, DOI: 10.1021/acs.nanolett.7b01592.